Chapter 6

Formability and Performance of Al-Zn-Mg-Cu Alloys with Different Initial Tempers in Creep Aging Process

Heng Li, Chao Lei and He Yang

Additional information is available at the end of the chapter

http://dx.doi.org/10.5772/intechopen.70849

Abstract

The initial temper may directly affect the deformation behavior and material performance in creep age forming (CAF) process. Five heat treatment states are selected as the initial tempers for CAF, namely, solution, peak-aging (T6), over-aging (T73), retrogression and re-solution. The formability and performance of an Al-Zn-Mg-Cu alloy with the above initial tempers in creep aging process are investigated via using creep and stress relaxation aging tests, mechanical property tests, corrosion resistance tests and microstructure analysis. The differences of formability are attributed to the inhibitions of different distributed matrix precipitates (MPts) on the dislocation movement, namely, the more coarsening the MPts is, the easier the dislocation movement. During creep aging process, the mechanical properties are improved for the solution, retrogression and re-solution tempers with fine MPts, but reduced for the T6 and T73 tempers due to coarsening of MPts. Since the distribution of grain boundary precipitates (GBPs) becomes discontinuous, the corrosion resistances of the creep aged specimens are enhanced for all initial tempers. Taking both mechanical properties and corrosion resistances into account, the re-solution temper may be a preferable choice to achieve high performance of the components beyond the precise shape in CAF.

Keywords: Al-Zn-Mg-Cu alloy, creep age forming, initial temper, precipitate, formability, mechanical property, corrosion resistance

1. Introduction

With the increasing demands for high-performance and light-weight in the components of aircraft and automobile, the Al-Zn-Mg-Cu (7xxx) series alloys have been widely used due to their high strength and relatively low density. The precipitation reaction is the leading strengthening mechanism in this class of alloys, and the precipitation sequence has been generally identified as supersaturated solid solution → Guinier-Preston (GP) zones → η' → η ($MgZn_2$) [1]. As a novel and promising forming technology, creep age forming (CAF) has been

developed and applied to manufacture large integral panel components, such as the upper wing panels of Airbus A380, and both the upper and lower wing skins of B-1B′ Long Range Combat Aircraft [2]. Compared to traditional manufacturing techniques, CAF has one of the most prominent advantage, namely, due to the simultaneity of creep deformation and age hardening, the shape forming process and the material strengthening process can be integrated into one single process, thus reducing the cost of manufacturing.

The complexity of CAF lies in the strong interaction coupling between creep and aging. Specifically, the precipitates generated in aging process will significantly hinder dislocation movement. Inversely, the dislocation density variation induced by creep deformation will affect the nucleation and growth of precipitates. Therefore, it is very difficult to precisely control the product shapes and material properties. Furthermore, it is well known that the Al-Zn-Mg-Cu alloys have many heat treatment states, and any one of the states can be the initial temper of the material used in CAF. Various initial tempers inevitably cause different couplings between creep and aging, and then make it difficult to precisely control the CAF process [3]. In order to acquire the high performance of formed components beyond the precise shape, it is very necessary to study the dependences of formability and performance on the initial tempers of Al-Zn-Mg-Cu alloys during CAF.

A lot of experimental studies mainly aimed at finding out the effects of processing parameters on CAF. Arabi Jeshvaghani et al. [4, 5] studied the effects of time and temperature on microstructure evolution of 7075 aluminum alloy sheet during CAF, and observed the transmission electron microscope (TEM) bright field images of matrix precipitates (MPts) and grain boundary precipitates (GBPs) in the formed samples after different forming periods, 6, 12 and 24 h, respectively. Guo et al. [6] found that the external elastic tensile stress promotes the formation of precipitates and shortens the aging period of an Al-Zn-Mg-Cu alloy. Lin et al. [7] found that the main precipitates of Al-Zn-Mg-Cu alloys during creep aging process are metastable η′ and stable η phases, and both of them are sensitive to the external factors, such as applied stress and aging temperature. Chen et al. [8] found that the applied stress induces the coarsening of precipitates in 7050 aluminum alloy during creep aging process, and both yield strength (YS) and tensile strength (TS) of the creep aged samples are lower than those of the stress-free aged samples. Lin et al. [9] studied the relationship between exfoliation corrosion (EXCO) sensitivity and creep aging process conditions, and found that the EXCO resistance of an Al-Zn-Mg-Cu alloy first increases and then decreases with the increase in stress and temperature. Li et al. [10] investigated the creep aging behaviors of an Al-Cu-Li alloy with different initial tempers, namely, solution, under-aging and peak-aging, and revealed there is a close relationship between creep mechanism and initial temper.

In view of the large springback occurred in the unloading process, many numerical studies mainly aimed at predicting springback after CAF to improve the forming precision. Based on the damage theory by Kowalewski et al. [11] and the conventional creep damage model [12], Ho et al. [13] proposed a unified creep constitutive model, and simulated the whole CAF process including loading, forming and unloading by using this constitutive model combined with the commercial finite element solver ABAQUS. Based on this work, Jeunechamps et al. [14] suggested a unified creep aging constitutive model considering the age hardening during

http://dx.doi.org/10.5772/intechopen.70849

CAF, in which the nucleation and growth of precipitates were related to the creep deformation. Lin et al. [15] introduced an integrated process to model stress relaxation, creep deformation, precipitation hardening and springback in CAF. Zhan et al. [16] developed a microstructure internal variables based creep aging constitutive model, which can describe the YS evolution through integrating the contribution of each hardening mechanism, namely dislocation hardening, age hardening and solution hardening.

It is noted that the initial tempers of aluminum alloys in above experiments and modeling are mostly solution temper, and the effects of various initial tempers on deformation and properties of Al-Zn-Mg-Cu series alloys in CAF are rarely reported. Therefore, in order to clearly understand the interaction between creep and aging, and achieve both high-precision forming and mechanical property improvement, this study focuses on investigating the effects of initial tempers on formability and performance of Al-Zn-Mg-Cu series alloys. In terms of creep deformation and stress relaxation, the formability of an Al-Zn-Mg-Cu alloy with various initial tempers under CAF conditions is evaluated firstly. Then, the evolution of microstructures and performance are revealed. Finally, based on the relations among creep deformation, material properties and microstructure evolution, the effects of initial tempers on formability and performance are discussed.

2. Experimental procedures

2.1. Specimen preparation and heat treatment for various initial tempers

A typical commercial 7050 aluminum alloy (AA7050) hot rolled plate with 30 mm thickness was used in this work, which belongs to the heat-treatable high strength Al-Zn-Mg-Cu series alloys. This alloy was provided by Northeast Light Alloy Co., Ltd., Harbin, China, and its chemical composition (wt.%) was verified by a SPECTRO MAXx direct-reading spectrometer, as listed in **Table 1**. The as-rolled Al-Zn-Mg-Cu alloys have been certified as containing coarse constituent particles (Al_7Cu_2Fe and Mg_2Si) and fine intermetallics ($MgZn_2$ and Al_2CuMg). The fine intermetallics can be dissolved by subsequent solution treatment, but the coarse constituent particles are quite stable and insoluble [17, 18]. The creep aging test specimens with the gauge length of 50 mm and thickness of 3 mm were machined out from the hot rolled plate by wire electrical discharge machining (WEDM) along the rolling direction, and their geometry and dimensions are shown in **Figure 1**.

In this work, five heat treatment states were selected as the material initial tempers in creep aging tests. The solution temper is the most widely used material initial temper in industrial CAF. The peak-aged (T6) and over-aged (T73) tempers are the most common delivery conditions of AA7050. Since the retrogression and re-aging (RRA) treatment can help Al-Zn-Mg-Cu

Zn	Mg	Cu	Zr	Ti	Fe	Si	Al
6.02	1.97	2.23	0.12	0.03	0.10	0.07	Bal.

Table 1. Chemical composition (wt.%) of as-received AA7050.

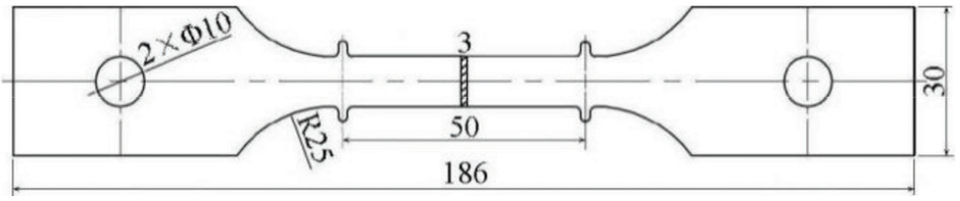

Figure 1. Geometry and dimensions of creep aging test specimens (unit: mm).

alloys to simultaneously achieve high mechanical properties and excellent corrosion resistance [19, 20], the retrogression temper is selected to be an initial temper. That is to say, the creep aging process will play the role of re-aging in RRA. Nevertheless, Lin et al. [21] pointed out that the narrow temperature-time window in RRA does not apply to the thick plate. Thus, the re-solution and re-aging (RSRA) treatment with wider temperature-time window has been developed in response to the similar effect as RRA, and the re-solution temper is chosen as one of the initial tempers in this study [22]. **Figure 2** shows various heat treatment procedures conducted to obtain the designed initial tempers of AA7050.

- For the solution temper, the as-rolled material was subjected to a solution treatment at 470°C for 50 min and subsequent water quenching.
- The T6 temper was obtained by a peak-aging treatment at 120°C for 24 h.
- For the retrogression temper, the specimen with T6 temper had endured a retrogression treatment at 200°C for 5 min in a salt bath.
- The T73 temper was obtained by a two-step aging at 115°C for 8 h and then 165°C for 16 h.
- For the re-solution temper, the specimen with T73 temper went through a re-solution treatment including hot insulation at 470°C for 50 min and rapid water quenching.

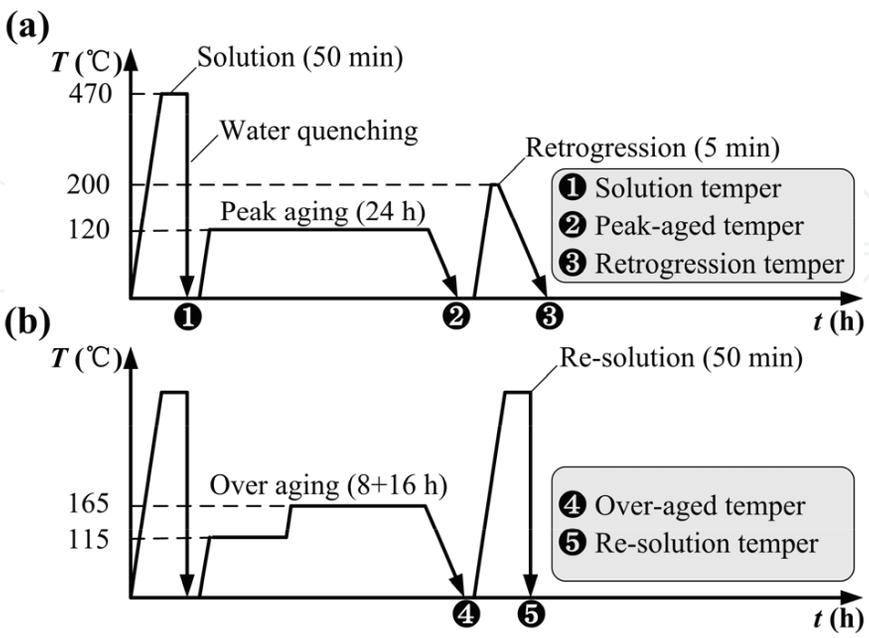

Figure 2. Heat treatment procedures of AA7050 for obtaining various initial tempers: (a) solution, T6 and retrogression; (b) T7 and re-solution.

2.2. Creep aging and stress relaxation aging tests

The creep aging and stress relaxation aging tests were carried out on a 100 kN electronic creep testing machine with special thermal environmental chamber. In the chamber, the temperature fluctuation can be controlled to less than 1°C. The tests were conducted under the aging temperature of 165°C to obtain more significantly creep deformation than those under the conventional T6 treatment temperature of 120°C. The applied stress of 250 MPa was within the typical stress range in the actual CAF process [23], and loaded on the specimen according to a loading speed of 0.5 mm/min. Meanwhile, in order to avoid the serious over-aging, the testing time is reduced to 18 h from the T6 treatment time of 24 h [24].

The installation position of the specimen was located in the middle of the chamber. The specimen was heated to 165°C, and then holds for 10 min before loading. The temperature was monitored at three positions around the specimen, namely, the two ends and the middle of the specimen. The change of gauge length on the specimen was measured by a high-precision (5×10^{-4} mm) grating line displacement transducer.

- In creep aging tests, the applied stress of 250 MPa remained the same throughout the creep deformation process. When the tests went on for 6 h, some tests were stopped as interrupted tests to investigate the evolution of microstructure and performance during CAF process.
- In stress relaxation aging tests, the applied stress of 250 MPa was a starting stress to obtain a given strain which remained unchanged during the stress relaxation process.

2.3. Microstructure characterizations and performance tests

The nano-sized precipitate microstructures were analyzed using the TECNAL G2 F30 transmission electron microscope (TEM). A slice was cut from the creep aged or stress relaxation aged specimen by WEDM, and then sanded to 60 μm thickness using sandpaper. Some 3 mm diameter round pieces as the TEM specimens were blanked from the slice and twin-jet electro-polished in a solution of 20% perchloric acid and 80% ethanol (in volume) at −20°C and 20 V. The quantitative analysis of the MPts in TEM bright field image was conducted by the Image-Pro Plus 6 software with no less than five images counted for each specimen.

The performance of the creep aged and stress relaxation aged specimens examined in this study is YS, TS, elongation, hardness, electrical conductivity, EXCO resistance and stress corrosion crack (SCC) resistance. The YS, TS and elongation were tested by the tensile tests conducted on a MTS CMT5205 electronic universal testing machine under the tensile speed of 2 mm/min. The hardness tests were carried out using a digital micro-hardness tester. Also, 10 tests were performed on each specimen to calculate an average. The electrical conductivity was measured by the eddy current method. The SCC resistances were evaluated using the slow strain rate tests (SSRT) in a corrosive environment of 3.5% NaCl. The accelerated EXCO tests were carried out in a classic etchant consisted of 4.0 M NaCl, 0.5 M KNO_3 and 0.1 M HNO_3. The specimen surfaces of EXCO tests were studied using a JEOL JCM-6000 scanning electron microscope (SEM).

3. Results

3.1. Creep deformation, stress relaxation and formability

Figure 3 shows the creep deformation and stress relaxation behaviors of AA7050 with different initial tempers during creep aging and stress relaxation aging tests. In the constant-stress creep aging tests under 165°C and 250 MPa, the specimens with four initial tempers of solution, T6, retrogression and re-solution all exhibit typical creep behaviors including primary and steady stages, but the specimen with initial temper of T73 represents primary and tertiary stages, as shown in **Figure 3(a)**. The primary creep stage lasts about 0.5 h and has a decrease of creep rate. After that, the strain hardening caused by creep and the softening caused by structural recovery gradually achieve a balance, and then the creep process enters into the second stage, namely steady creep stage. Four creep strain curves almost overlap with each other before the first half of steady stage. The bifurcation on those curves appears about 6 h later. After creep aging tests of 18 h, the largest creep strain is obtained in the T73 temper, and the least creep strain appears in the re-solution temper. However, the specimens with initial tempers of T6 and T73 apparently enter the tertiary creep stage. It means that the interior of material has generated a lot of microdefects, which is no longer applicable to the manufacture of aviation components. Using the amount of creep strain to evaluate the formability, the consequence of the creep aging formability of the specimens with three initial tempers except T6 and T73 is retrogression > solution > re-solution. The final creep strain for the retrogression temper is about 1.21 and 1.34 times than that for the solution and the re-solution tempers, respectively.

A practical CAF process usually involves loading, forming, and unloading stages. The workpiece is fitted closely with the tool surface after loading stage, and its shape will remain unchanged in subsequent forming stage until unloading. In the forming process, part of the elastic deformation is transformed into an irreversible plastic (creep) deformation, and the stress gradually decreases. Thus, the CAF process is more like a stress relaxation process [25]. After the forming stage, the stress cannot be released completely. The residual stress causes the workpiece to produce a larger springback in the unloading stage. In general, the larger stress relaxation signifies the better formability of CAF. **Figure 3(b)** shows the stress relaxation curves of AA7050 with different initial tempers during the stress relaxation aging tests under

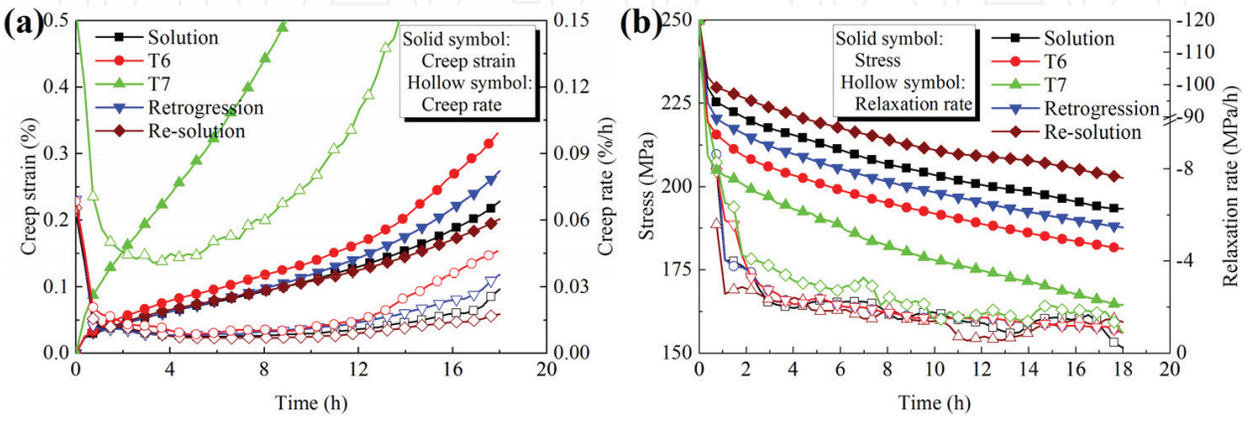

Figure 3. Creep deformation and stress relaxation behaviors of AA7050 with different initial tempers: (a) curves of creep strain and creep rate; (b) curves of stress relaxation and relaxation rate.

http://dx.doi.org/10.5772/intechopen.70849

165°C and initiating stress of 250 MPa. The stress decreases for the five initial tempers are very sharp in the beginning, and turn to slow in the later period. The T73 temper has the largest relaxed stress, and the re-solution temper has the smallest relaxed stress. Comparing the magnitude of relaxed stress, it can be seen that the order of formability of the specimens with five initial tempers is T73 > T6 > retrogression > solution > re-solution. This result is consistent with the above conclusion of creep aging tests. An inference can be drawn that the root cause of stress relaxation is the occurrence of creep deformation.

3.2. Evolution of microstructures

3.2.1. Matrix precipitates

In the precipitation reaction of the Al-Zn-Mg-Cu alloys under the CAF condition, the metastable η′ phase and stable η phase are main precipitates and formed in the supersaturated aluminum matrix. **Figure 4** shows the MPt microstructures of AA7050 with different initial tempers before the creep aging tests. Both η′ and η phases can affect the creep behavior, so there is no special distinction between the types of precipitates. **Figure 4(a)** shows that there is no obvious precipitate in the alloy with solution temper. **Figure 4(b)** displays many fine precipitates with average radius of 2.8 nm and number density of 1.7×10^{18} cm^{-3} evenly distributed in the matrix of alloy with T6 temper. **Figure 4(c)** represents some coarse precipitates with average radius of 4.3 nm and number density of 6.3×10^{17} cm^{-3} uniformly

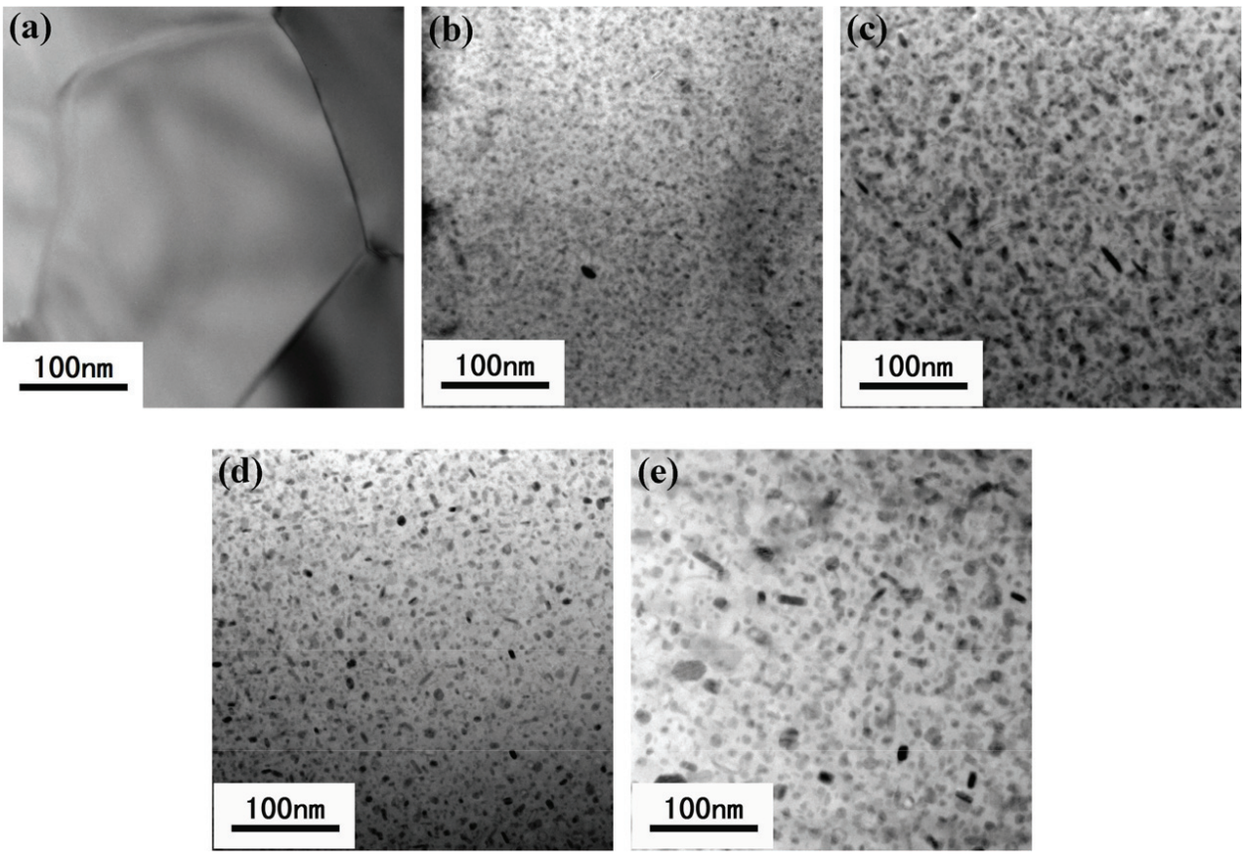

Figure 4. TEM images of MPts of AA7050 with different initial tempers before creep aging tests: (a) solution; (b) T6; (c) T73; (d) retrogression; (e) re-solution.

distributed in the matrix of over-aged alloy. Through retrogression treatment for the peak-aged alloy, parts of MPts has been dissolved, and the residual MPts have the average radius of 3.2 nm and number density of 5.5×10^{17} cm^{-3}, as shown in **Figure 4(d)**. Therefore, it can be seen that the short-time retrogression treatment cannot dissolve the whole precipitates. **Figure 4(e)** shows the sporadic MPts distributed in the matrix of re-solution treated alloy, and the average radius and number density of these precipitates are 4.8 nm and 7.9×10^{14} cm^{-3}, respectively. This suggests that due to the higher temperature and longer insulation time of the re-solution treatment, plenty of precipitates in over-aged alloy are dissolved, and only few precipitates are remained and coarsened.

In **Figure 3**, some creep curves are almost overlapping in the early stage of the creep aging process. It can be inferred that the initial microstructures have little effect on the creep deformation. The different creep rates appear in about 6 h, and the reason can be attributed to the different precipitate microstructures of AA7050 with different initial tempers after creep aging tests of 6 h. It also can be seen that, in the creep aging tests, the minimum creep rates appear at around 6 h, which indicates that the precipitate microstructures have the strongest effect on creep deformation at this time.

In the creep aging process, due to the precipitation reaction, the size of the MPts is greatly changed. **Figure 5** shows the MPt microstructures of AA7050 with different initial tempers after

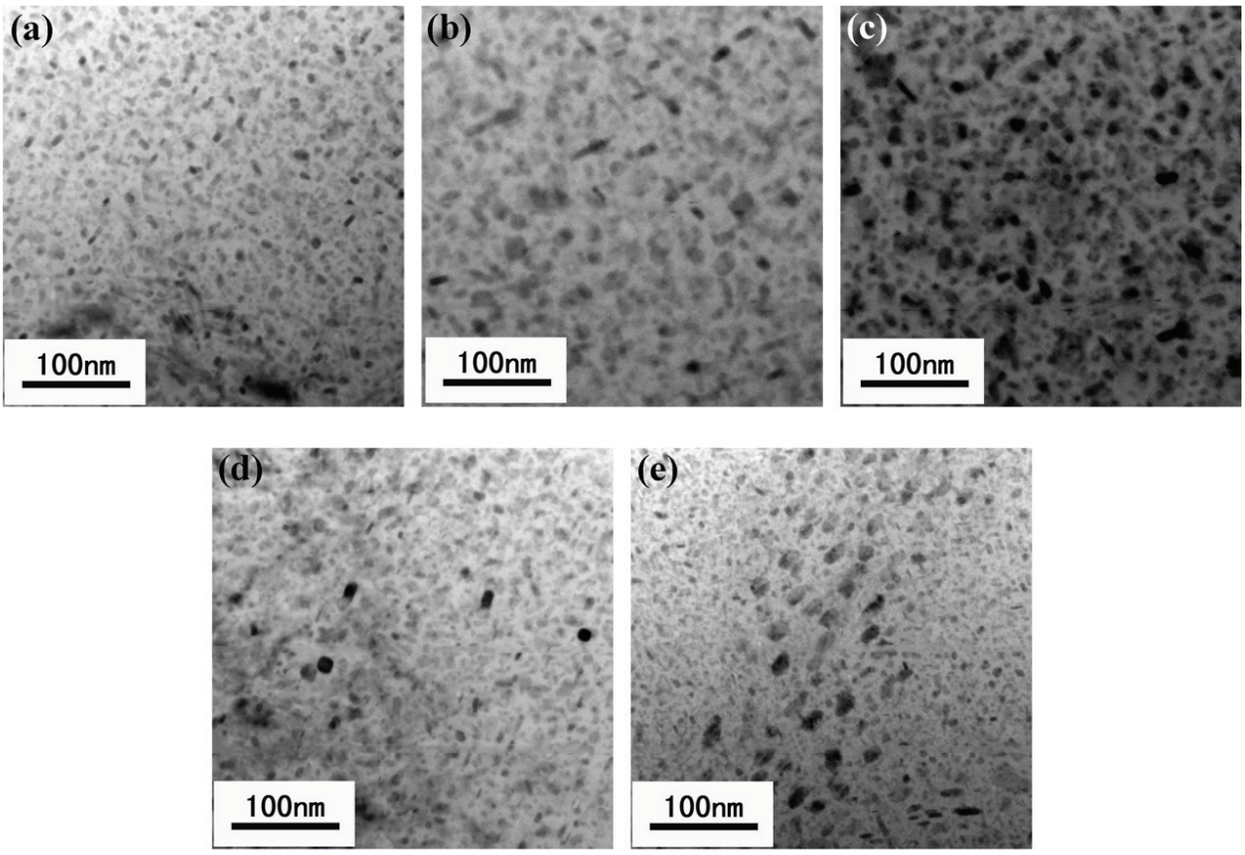

Figure 5. TEM images of MPts of AA7050 with different initial tempers after creep aging tests of 6 h: (a) solution; (b) T6; (c) T73; (d) retrogression; (e) re-solution.

http://dx.doi.org/10.5772/intechopen.70849

the creep aging tests of 6 h. As shown in **Figure 5(a)**, there are a lot of fine precipitates with an average radius of 3.5 nm. **Figure 5(b)** and **(c)** presents that the MPts in the alloy with T6 and T73 tempers grow, respectively, to 6.3 and 7.4 nm. **Figure 5(d)** represents the microstructure evolution of the retrogression treated specimen, and all previous MPts are coarsened to an average radius of 4.6 nm. This image clearly shows that, after the creep aging tests of 6 h, the size of MPts in the alloy with retrogression temper is bigger than that with solution temper. In **Figure 5(e)**, since most of MPts in T73 temper are dissolved by the previous re-solution treatment, after the creep aging tests of 6 h, a lot of new precipitates with small size are re-precipitated in the matrix of the alloy with re-solution temper accompanied by the coarsening of previous residual precipitates. In calculating the size of the new precipitates, the initial average radius of previous residual precipitates is set to be a threshold value. Excluding the precipitates which are bigger than the threshold radius of 4.8 nm, the average radius of new precipitates is 2.9 nm. It can be seen that the size of new MPts of re-solution tempered specimen is the smallest in the specimens with five initial tempers after the creep aging tests of 6 h.

3.2.2. Grain boundary precipitates

Figure 6 shows the GBP microstructures of AA7050 with different initial tempers before the creep aging tests. As shown in **Figure 6(a)**, there is no obvious precipitate on the grain

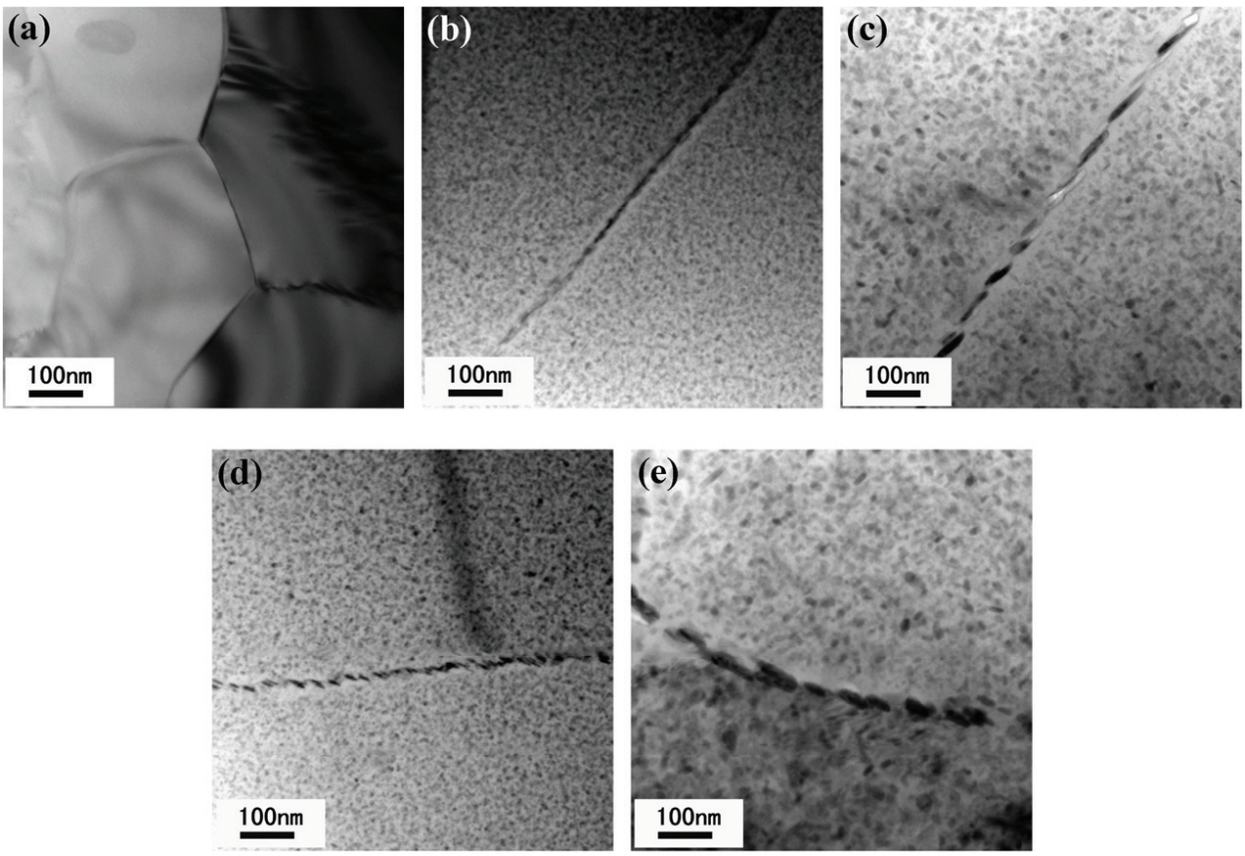

Figure 6. TEM images of GBPs of AA7050 with different initial tempers before creep aging tests: (a) solution; (b) T6; (c) T73; (d) retrogression; (e) re-solution.

boundary of the specimen with solution temper. This indicates that the intermetallics of as-rolled AA7050 have been dissolved by the solution treatment. **Figure 6(b)** shows that the specimen with T6 temper has continuously distributed GBPs. By comparing **Figure 6(b)** and **(d)**, it can be found that the alloy with retrogression temper has slightly discontinuous GBPs than that with T6 temper. This indicates that the role of short-time retrogression treatment on the dissolution of precipitates is limited. **Figure 6(c)** shows that the specimen with T73 temper has discontinuous GBPs with large spacing. The comparison between **Figure 6(c)** and **(e)** shows that, through re-solution treatment, the GBPs become smaller in size. It demonstrates that the re-solution treatment not only dissolve the MPts but also the GBPs.

Figure 7 represents the GBP microstructures of AA7050 with different initial tempers after the creep aging tests. The GBP microstructures of the specimen with initial temper of solution is similar to that of T6 temper, namely continuously distributed GBPs, as shown in **Figure 7(a)**. **Figure 7(b)** shows that the GBPs in the specimen with T6 temper translate from continuous to discontinuous in the creep aging tests. **Figure 7(c)–(e)** reveal the growth of previous GPBs in the specimens with initial temper of T73, retrogression and re-solution, resulting in more discontinuous grain boundary structures. Among them, the specimen with T73 temper has the largest sized GBPs with the widest spacing.

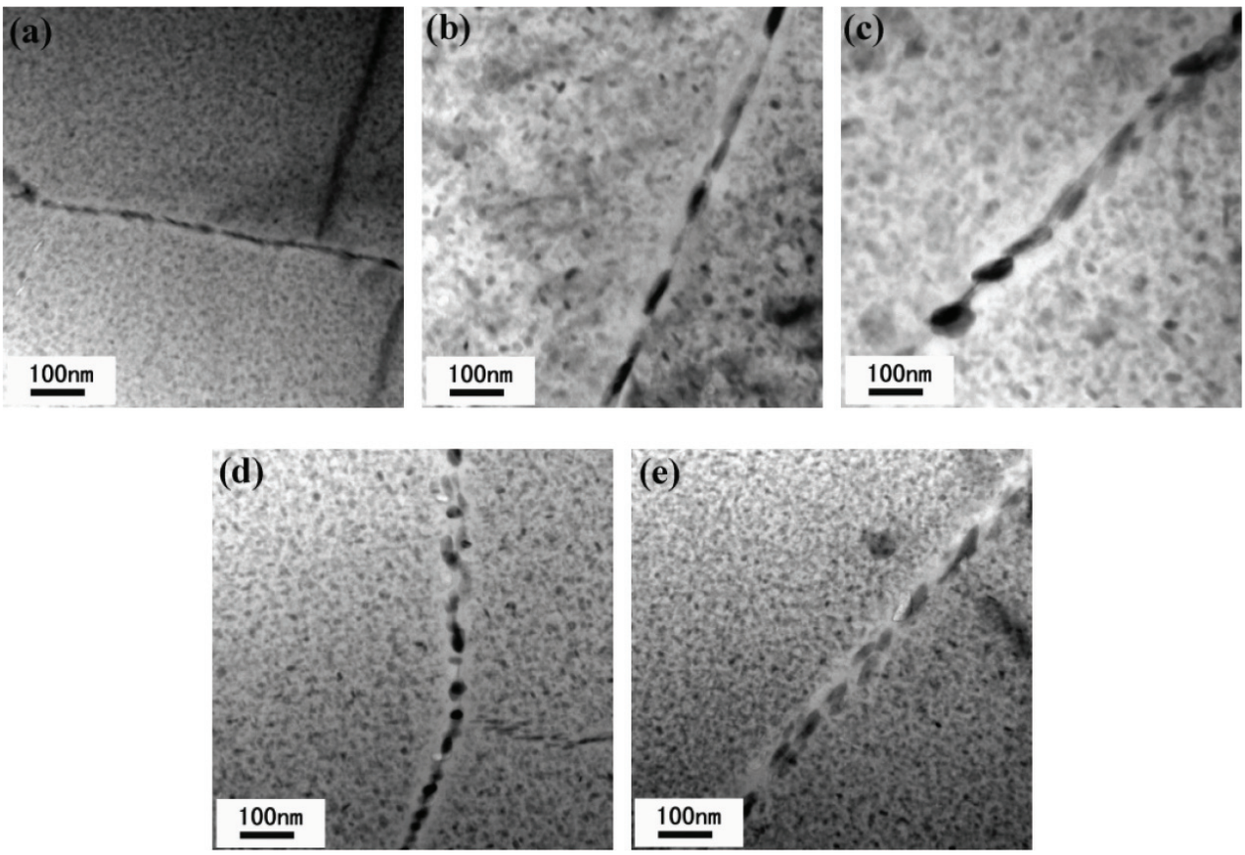

Figure 7. TEM images of GBPs of AA7050 with different initial tempers after creep aging tests: (a) solution; (b) T6; (c) T73; (d) retrogression; (e) re-solution.

http://dx.doi.org/10.5772/intechopen.70849

3.3. Evolution of material performance

3.3.1. Mechanical properties and electrical conductivity

Figure 8(a) illustrates the YS, TS and elongation of AA7050 with different initial tempers before and after creep aging tests. It can be seen that the mechanical strength of the specimen with initial temper of solution obtains the maximized promotion in the creep aging tests. On the contrary, the mechanical strengths of the specimens with initial tempers of T6 and T73 reduce. Compared with solution and re-solution tempers, the specimen with initial temper of retrogression has the highest strength before creep aging. However, the mechanical strength of this specimen is significantly lower after creep aging. Its YS and TS are approximately 18% and 9% lower than those of the creep aged specimen with initial temper of solution. The YS and TS of the creep aged specimen with initial temper of re-solution are only 4% and 2% lower than those of solution temper. In addition, the sorting of elongations is the opposite to that of mechanical strengths, namely T73 > T6 > retrogression > re-solution > solution.

Figure 8(b) shows the hardness and electrical conductivity of AA7050 with various initial tempers before and after the creep aging tests. The contrast situation of hardness is identical to that of strength. Tsai and Chuang [26] determined that the electrical conductivity of aluminum alloy may serve as an indicator of SCC resistance, so the electrical conductivity tests were carried out as the circumstantial evidence for subsequent SCC resistance tests. It can be see that, for each initial temper, the electrical conductivity of specimen increases with time. At the end of creep aging process, the sequence of electrical conductivity is T73 > T6 > re-solution > retrogression > solution.

3.3.2. SCC and EXCO resistances

In the SSRT, the index r_{tf} is commonly used to evaluate the SCC resistance and calculated by [22]:

$$r_{tf} = \frac{t_{fe}}{t_{fc}} \tag{1}$$

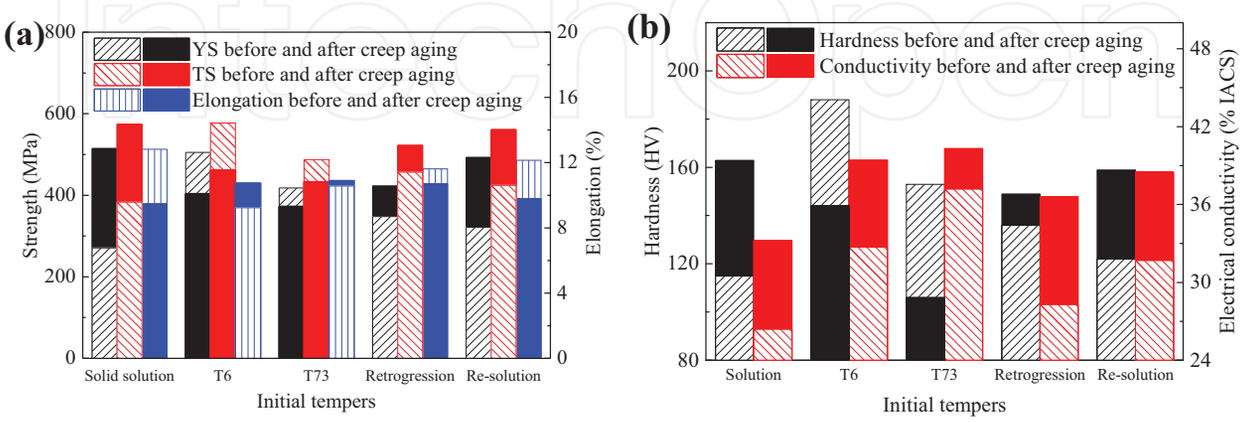

Figure 8. Performance change of AA7050 with different initial tempers before and after creep aging tests: (a) strength and elongation; (b) hardness and electrical conductivity.

where t_{fe} is the time of specimen fracture in the corrosive environment and t_{fc} is the corresponding time in the atmospheric environment. The closer the r_{tf} value is to 1, the better the SCC resistance.

Table 2 lists the r_{tf} values of creep aged AA7050 with different initial tempers. After creep aging process, the specimens with initial tempers of T6, T73 and re-solution have better SCC resistance than those with initial tempers of solution and retrogression.

In the accelerated EXCO tests, the corrosion products gradually break away from the specimen surface. **Figure 9** displays the surface morphology of the creep aged specimens continuously immersed in the EXCO solution for 48 h. The creep aged specimen with initial temper of solution has been seriously corroded, and a mass of corrosion products is detached from the metal surface. There are negligible corrosion phenomena which occur in the creep aged specimens with initial tempers of T6 and T73. For the retrogression temper, there are some cracks appeared on the metal surface. Conversely, some tiny cracks can be found on the surface of the creep aged specimen with initial temper of re-solution.

Using EXCO grade to evaluate the degree of corrosion, the total EXCO behavior can be classified into six grades, namely free of obvious corrosion (expressed as N), slight pitting (P), growing pitting (EA), slight surface crack (EB), corrosion peeling and blister (EC) and corrosion product

Initial temper	Solution	T6	T73	Retrogression	Re-solution
r_{tf} value	0.724	0.972	0.987	0.903	0.956

Table 2. r_{tf} values of AA7050 with different initial tempers after creep aging tests.

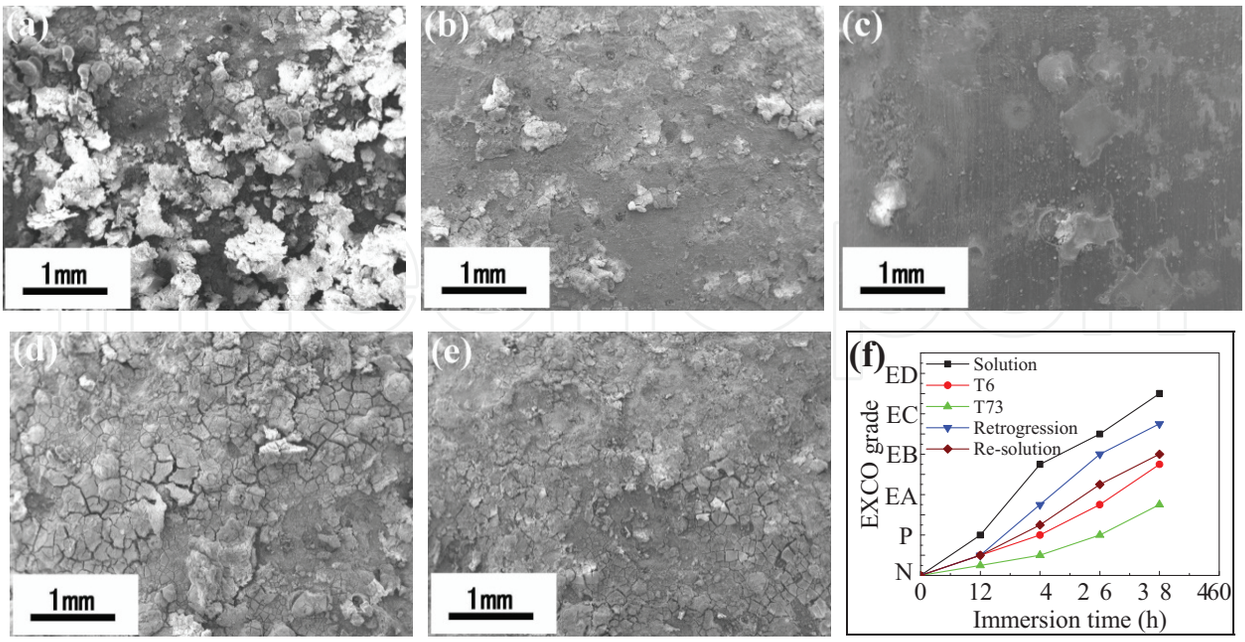

Figure 9. EXCO morphologies of creep aged AA7050 with different initial tempers: (a) solution; (b) T6; (c) T73; (d) retrogression; (e) re-solution; (f) corresponding EXCO grade evolution.

http://dx.doi.org/10.5772/intechopen.70849

shedding (ED). **Figure 9(f)** shows the EXCO grade evolution of the creep aged AA7050 with various initial tempers during the EXCO tests, and it can be found that the degree of EXCO aggravates with immersion time.

4. Discussion

4.1. Issue of formability

4.1.1. Deformation mechanism

In CAF process, the creep strain rate can be described by [27, 28]:

$$\dot{\varepsilon}_c = A\sigma^n \exp\left(-\frac{Q}{RT}\right) \tag{2}$$

where σ is the instantaneous stress and A, n, Q, R and T are material constant, stress exponent, deformation activation energy, universal gas constant and Kelvin temperature, respectively.

Translating the both sides of Eq. (2) into logarithmic form, the strain rate-stress double logarithmic curves as shown in **Figure 10**. The data of strain rate and stress are taken from the stress relaxation curves in **Figure 3**. Just to be clear, because the creep deformation of T6 and T73 tempers enters into the tertiary stage, these two tempers are not take into account of the discussion for deformation mechanism.

Figure 10(a) shows that each strain rate-stress double logarithmic curve consists of three straight lines corresponding to three different stages in the stress relaxation aging process, namely primary, transition and steady stages. The inflection point between two intersecting straight lines indicates that there is a threshold stress occurred in the transformation of two adjacent stages [25]. Since the threshold stress is the minimum stress required for creep deformation, the different threshold stresses can reflect the differences of CAF formability.

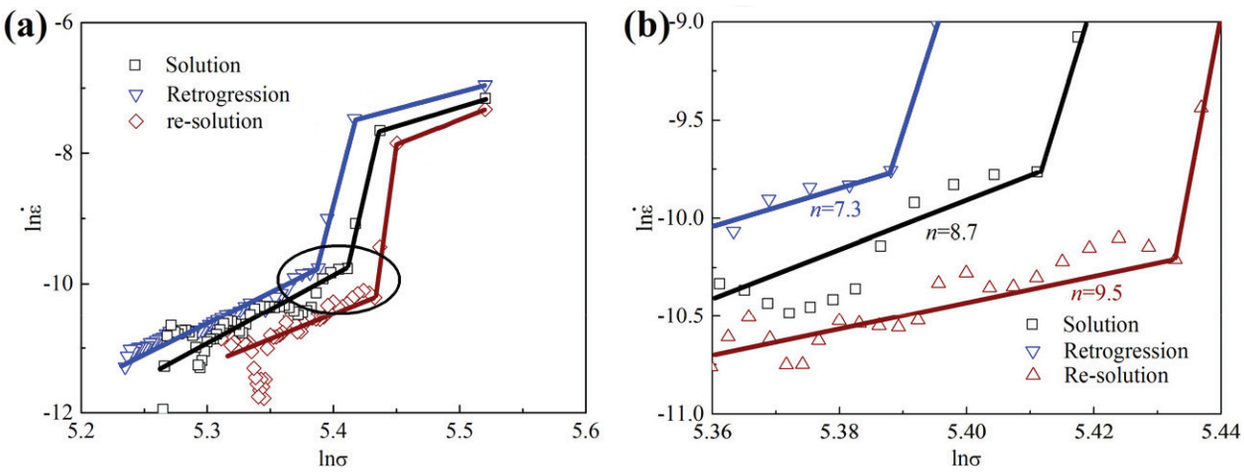

Figure 10. Strain rate versus stress double logarithmic curves of AA7050 with different initial tempers during stress relaxation aging tests: (a) total curves; (b) local enlargement in the circle.

Initial temper	Solution	Retrogression	Re-solution
Upper threshold stresses (MPa)	229.8	225.1	232.9
Lower threshold stresses (MPa)	223.9	218.7	228.8

Table 3. Upper and lower threshold stresses of AA7050 with various initial tempers in CAF at 165°C.

In other words, the smaller threshold stress means the better formability. **Table 3** lists the upper and lower threshold stresses in CAF at 165°C for the specimens with solution, retrogression and re-solution tempers. When the stress drops lower than the upper threshold stress, the strain rate reduces sharply, and the CAF process enters into the transition stage from the primary stage. When the stress falls below the lower threshold stress, the forming process enters into the final steady stage. Whether upper or lower threshold stresses, the order of various initial tempers is re-solution > solution > retrogression. It means that the retrogression temper corresponds to the best CAF formability.

The dominant mechanism of creep deformation can be reflected from the stress exponent n [28], which can be calculated through fitting the slopes of strain rate-stress double logarithmic curves of the steady stage in stress relaxation process. **Figure 10(b)** shows that the values of stress exponent n in the steady stage CAF at 165°C for the AA7050 with solution, retrogression and re-solution tempers are 8.7, 7.3 and 9.5, respectively. The value of n less than 2 indicates that the creep deformation mechanism mainly is diffusion. While the value of n greater than 4 means that the creep deformation is controlled by dislocation movement, including dislocation slip and dislocation climb [29]. It follows that the dominant deformation mechanism of AA7050 in the creep aging process under 165°C is dislocation creep.

4.1.2. Formability and MPts

Since the dislocation movement is affected by the size and distribution of the MPts, there is a direct relationship between the precipitate microstructures and formability of AA7050 during CAF. By comparing the precipitate microstructures of the specimens with different initial tempers after the creep aging tests of 6 h in **Figure 5**, it is shown that the specimen with initial temper of T73 has the largest MPts, and the specimen with initial temper of re-solution has the smallest MPts. It well known that the small-sized precipitates will be cut by dislocation during plastic deformation process of metal, while the big-sized precipitates will be bypassed. Thus, the AA7050 with initial temper of T73 has the best formability because of its big-sized precipitates are bypassed by the moving dislocation, but the alloy with initial temper of re-solution has the worst formability since its small-sized precipitates pin the dislocation [30].

4.2. Issue of performance

4.2.1. Mechanical properties and MPts

It is generally known that the main influencing factor for mechanical properties of the heat-treatable aluminum alloys is the size of MPts. Since its fine MPts similar to the T6 temper, the specimen with initial temper of solution has the highest YS and TS after creep aging tests. Because there is only the coarsening action of MPts, the mechanical strength of the specimens

http://dx.doi.org/10.5772/intechopen.70849

with initial tempers of T6 and T73 has actually lowered. In the creep aged specimen with initial temper of re-solution, the re-precipitation takes place in the creep aging process, thus the fine MPts leads to the higher strength which close to the strength of T6.

4.2.2. Corrosion resistance and GBPs

The corrosion resistance of Al-Zn-Mg-Cu alloys is directly determined by grain boundary structure. The continuously distributed GBPs can create an anodic corrosion channel, where a galvanic reaction will occur between the GBPs as anode and the aluminum matrix as cathode in a corrosive environment [31]. For the solution and retrogression tempers, since their creep aged specimens have continuous GPBs, these two tempers show higher sensitivity of EXCO and SCC. Conversely, the discontinuous GPBs of the creep aged specimens with initial temper of T6, T73 and re-solution cannot form effective anodic corrosion channel, thus these three tempers have better corrosion resistances. The SCC mechanism of the Al-Zn-Mg-Cu alloys is also considered to be the effect of hydrogen embrittlement except the anodic dissolution [21].

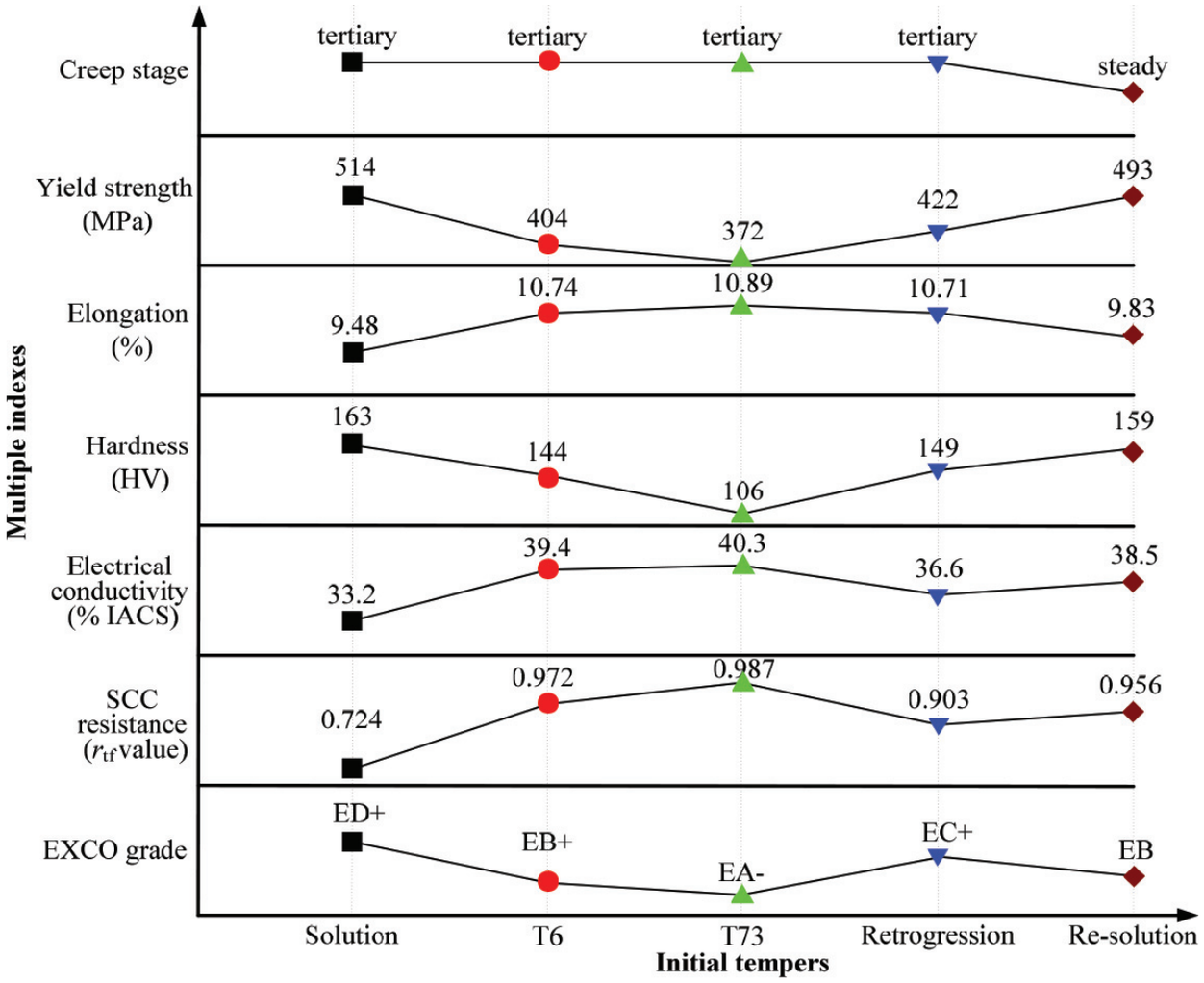

Figure 11. Multiple performance indexes of creep aged AA7050 with different initial tempers.

The small and continuous GBPs in solution and retrogression tempers cannot capture hydrogen atoms, then the SCC easily occurs on the grain boundary where concentrated a bunch of hydrogen atoms. Rather, the large and discontinuous GBPs in T6, T73 and re-solution tempers as the pitfalls of hydrogen atoms avoid the mass concentration of hydrogen atoms in the grain boundary, leading to the low SCC sensitivity.

4.3. Comprehensive evaluation by multiple indexes

Figure 11 displays the various material performances of AA7050 with various initial tempers, which are tested 18 h under creep aging tests conditions of 165°C and 250 MPa. When the tests comes to the end, only the specimen with initial temper of re-solution is absolutely still in the steady creep stage. This shows that it has the potential to sustain a longer CAF period. The mechanical properties of the creep aged specimen with initial temper of re-solution are very close to those of solution temper as the best case, and much more than those of T6, T73 and retrogression. Furthermore, the corrosion resistances of the creep aged specimen with initial temper of re-solution are very close to the best case in T73 temper.

Taking the both requirements of forming precision and material performance into account, a conclusion can be drawn by comparing the multiple indicators shown in **Figure 11**. The re-solution is the best choice for the initial temper of Al-Zn-Mg-Cu alloys in CAF under the given conditions, that is, the temperature of 165°C and the stress of 250 MPa.

5. Conclusions

In terms of the creep deformation and stress relaxation, as well as corresponding properties tests and microstructure observations, the effects of initial tempers on the creep aging formability and performance of an Al-Zn-Mg-Cu alloy (AA7050) have been studied under CAF conditions. The main findings can be summarized as follows:

1. Using various heat treatment methods, five material states of AA7050 are obtained to serve as initial tempers for CAF, namely, solution, T6, T73, retrogression and re-solution. The microstructure analyses show that there is no obvious MPts in the alloy with solution temper. The retrogression temper is transformed from T6 temper through retrogression treatment which makes slight reduction of MPts density and discontinuous distribution of GBPs. The re-solution temper is converted from T73 temper by re-solution treatment which fully dissolves the MPts and makes the GBPs smaller.

2. The T73 temper has the best formability, and the worst presents in the re-solution temper. Through calculating the stress exponents, it can be seen that the CAF of AA7050 under the given thermal-mechanical conditions is mainly controlled by dislocation creep. The TEM observations of the specimens after the creep aging tests of 6 h show that the T73 temper has the biggest sized MPts which can be bypassed by the moving dislocation, thus it has the best formability; the reason of the worst formability appeared in re-solution temper is that the alloy has the smallest sized MPts which can pin down the moving dislocation.

3. The mechanical properties of the creep aged specimens with various initial tempers are different. After creep aging, the specimens with initial tempers of solution and re-solution show almost same high mechanical properties than that of T6, T73 and retrogression. Its reason is that the creep aged specimens with initial tempers of solution and re-solution has fine and homogeneous MPts, while the MPts of the creep aged specimens with initial tempers of T6, T73 and retrogression grow up obviously. The discontinuous GBPs lead to the better EXCO and SCC resistance of the creep aged specimens with initial tempers of T6, T73 and re-solution. Conversely, the continuous GBPs result in the higher corrosion susceptibility of the creep aged specimens with initial tempers of solution and retrogression.
4. In order to achieve the dual objective of precise forming and performance improvement, the comprehensive assessment on multiple performance indexes indicates that the re-solution is the best choice for the initial temper of Al-Zn-Mg-Cu alloys in CAF under the given conditions. Re-solution temper has the potential to withstand long forming period and can bring excellent mechanical properties and corrosion resistances.

Acknowledgements

The authors would like to thank the National Natural Science Foundation of China for Key Program (51235010), the National Science Fund for Excellent Young Scholars (51522509), the Fundamental Research Funds for the Central Universities (3102014KYJD001), the Marie Curie International Research Staff Exchange Scheme (IRSES, MatProFuture, project no: 318968) within the 7th EC Framework Programme (FP7) and the 111 Project (B08040) for their financial supports.

Author details

Heng Li*, Chao Lei and He Yang

*Address all correspondence to: liheng@nwpu.edu.cn

State Key Laboratory of Solidification Processing, School of Materials Science and Engineering, Northwestern Polytechnical University, Xi'an, China

References

[1] Sha G, Cerezo A. Early-stage precipitation in Al-Zn-Mg-Cu alloy (7050). Acta Materialia. 2004;**52**:4503-4516. DOI: 10.1016/j.actamat.2004.06.025

[2] Zhan LH, Lin JG, Dean TA. A review of the development of creep age forming: Experimentation, modelling and applications. International Journal of Machine Tools & Manufacture. 2011;**51**:1-17. DOI: 10.1016/j.ijmachtools.2010.08.007

[3] Lei C, Yang H, Li H, Shi N, Fu J, Zhan LH. Dependence of creep age formability on initial temper of an Al-Zn-Mg-Cu alloy. Chinese Journal of Aeronautics. 2016;**29**:1445-1454. DOI: 10.1016/j.cja.2016.04.022

[4] Arabi Jeshvaghani R, Emami M, Shahverdi HR, Hadavi SMM. Effects of time and temperature on the creep forming of 7075 aluminum alloy: Springback and mechanical properties. Materials Science and Engineering A. 2011;**528**:8795-8799. DOI: 10.1016/j.msea.2011.08.025

[5] Arabi Jeshvaghani R, Shahverdi HR, Hadavi SMM. Investigation of the age hardening and operative deformation mechanism of 7075 aluminum alloy under creep forming. Materials Science and Engineering A. 2012;**552**:172-178. DOI: 10.1016/j.msea.2012.05.027

[6] Guo W, Yang M, Zheng Y, Zhang XS, Li H, Wen XY, Zhang JW. Influence of elastic tensile stress on aging process in an Al-Zn-Mg-Cu alloy. Materials Letters. 2013;**106**:14-17. DOI: 10.1016/j.matlet.2013.04.095

[7] Lin YC, Jiang YQ, Chen XM, Wen DX, Zhou HM. Effect of creep-aging on precipitates of 7075 aluminum alloy. Materials Science and Engineering A. 2013;**588**:347-356. DOI: 10.1016/j.msea.2013.09.045

[8] Chen JF, Zhen L, Jiang JT, Yang L, Shao WZ, Zhang BY. Microstructures and mechanical properties of age-formed 7050 aluminum alloy. Materials Science and Engineering A. 2012;**539**:115-123. DOI: 10.1016/j.msea.2012.01.067

[9] Lin YC, Jiang YQ, Zhang XC, Deng J, Chen XM. Effect of creep-aging processing on corrosion resistance of an Al-Zn-Mg-Cu alloy. Materials and Design. 2014;**61**:228-238. DOI: 10.1016/j.matdes.2014.04.054

[10] Li Y, Shi Z, Lin J, Yang YL, Huang BM, Chung TF, Yang JR. Experimental investigation of tension and compression creep-ageing behaviour of AA2050 with different initial tempers. Materials Science and Engineering A. 2016;**657**:299-308. DOI: 10.1016/j.msea.2016.01.074

[11] Kowalewski ZL, Hayhurst DR, Dyson BF. Mechanisms-based creep constitutive equations for an aluminium alloy. The Journal of Strain Analysis for Engineering Design. 1994;**29**:309-316. DOI: 10.1243/03093247v294309

[12] Lin J, Liu Y, Dean TA. A review on damage mechanisms, models and calibration methods under various deformation conditions. International Journal of Damage Mechanics. 2005;**14**:299-319. DOI: 10.1177/1056789505050357

[13] Ho KC, Lin J, Dean TA. Modelling of springback in creep forming thick aluminum sheets. International Journal of Plasticity. 2004;**20**:733-751. DOI: 10.1016/s0749-6419(03)00078-0

[14] Jeunechamps PP, Ho KC, Lin J, Ponthot JP, Dean TA. A closed form technique to predict springback in creep age-forming. International Journal of Mechanical Sciences. 2006;**48**:621-629. DOI: 10.1016/j.ijmecsci.2006.01.005

[15] Lin J, Ho KC, Dean TA. An integrated process for modelling of precipitation hardening and springback in creep age-forming. International Journal of Machine Tools and Manufacture. 2006;**46**:1266-1270. DOI: 10.1016/j.ijmachtools.2006.01.026

[16] Zhan LH, Lin J, Dean TA, Huang MH. Experimental studies and constitutive modelling of the hardening of aluminium alloy 7055 under creep age forming conditions. International Journal of Mechanical Sciences. 2011;**53**:595-605. DOI: 10.1016/j.ijmecsci.2011.05.006

[17] Xu DK, Rometsch PA, Birbilis N. Improved solution treatment for an as-rolled Al-Zn-Mg-Cu alloy. Part I. Characterisation of constituent particles and overheating. Materials Science and Engineering A. 2012;**534**:234-243. DOI: 10.1016/j.msea.2011.11.065

[18] Xu DK, Rometsch PA, Birbilis N. Improved solution treatment for an as-rolled Al-Zn-Mg-Cu alloy. Part II. Microstructure and mechanical properties. Materials Science and Engineering A. 2012;**534**:244-252. DOI: 10.1016/j.msea.2011.11.073

[19] Marlaud T, Deschamps A, Bley F, Lefebvre W, Baroux B. Evolution of precipitate microstructures during the retrogression and re-ageing heat treatment of an Al-Zn-Mg-Cu alloy. Acta Materialia. 2010;**58**:4814-4826. DOI: 10.1016/j.actamat.2010.05.017

[20] Oliveira AF Jr, de Barros MC, Cardoso KR, Travessa DN. The effect of RRA on the strength and SCC resistance on AA7050 and AA7150 aluminium alloys. Materials Science and Engineering A. 2004;**378**:321-326. DOI: 10.1016/j.msea.2004.02.052

[21] Lin JC, Liao HL, Jehng WD, Chang CH, Lee SL. Effect of heat treatments on the tensile strength and SCC-resistance of AA7050 in an alkaline saline solution. Corrosion Science. 2006;**48**:3139-3156. DOI: 10.1016/j.corsci.2005.11.009

[22] Lei C, Yang H, Li H, Shi N, Zhan LH. Dependences of microstructures and properties on initial tempers of creep aged 7050 aluminum alloy. Journal of Materials Processing Technology. 2017;**239**:125-132. DOI: 10.1016/j.jmatprotec.2016.07.004

[23] Ho KC, Lin J, Dean TA. Constitutive modelling of primary creep for age forming an aluminium alloy. Journal of Materials Processing Technology. 2004;**153-154**:122-127. DOI: 10.1016/j.jmatprotec.2004.04.304

[24] Guyot P, Cottignies L. Precipitation kinetics, mechanical strength and electrical conductivity of AlZnMgCu alloys. Acta Materialia. 1996;**44**:4161-4167. DOI: 10.1016/S1359-6454(96)00033-X

[25] Chen JF, Jiang JT, Zhen L, Shao WZ. Stress relaxation behavior of an Al-Zn-Mg-Cu alloy in simulated age-forming process. Journal of Materials Processing Technology. 2014;**214**:775-783. DOI: 10.1016/j.jmatprotec.2013.08.017

[26] Tsai TC, Chuang TH. Relationship between electrical conductivity and stress corrosion cracking susceptibility of Al 7075 and Al 7475 alloys. Corrosion Science. 1996;**52**:414-416. DOI: 10.5006/1.3292127

[27] Wang H, Wang QD, Yin DD, Yuan J, Ye B. Tensile creep behavior and microstructure evolution of extruded Mg-10Gd-3Y-0.5Zr (wt%) alloy. Materials Science and Engineering A. 2013;**578**:150-159. DOI: 10.1016/j.msea.2013.04.068

[28] Mostafa MM, Al-Ganainy GS, El-Khalek AMA, Nada RH. Steady-state creep and creep recovery during transformation in Al-Zn alloys. Physica B: Condensed Matter. 2003;**336**:402-409. DOI: 10.1016/s0921-4526(03)00318-1

[29] Mahmudi R, Roumina R, Raeisinia B. Investigation of stress exponent in the power-law creep of Pb-Sb alloys. Materials Science and Engineering A. 2004;**382**:15-22. DOI: 10.1016/j.msea.2004.05.078

[30] Guo W, Guo JY, Wang JD, Yang M, Li H, Wen XY, et al. Evolution of precipitate microstructure during stress aging of an Al-Zn-Mg-Cu alloy. Materials Science and Engineering A. 2015;**634**:167-175. DOI: 10.1016/j.msea.2015.03.047

[31] Li JF, Birbilis N, Li CX, Jia ZQ, Cai B, Zheng ZQ. Influence of retrogression temperature and time on the mechanical properties and exfoliation corrosion behavior of aluminium alloy AA7150. Materials Characterization. 2009;**60**:1334-1341. DOI: 10.1016/j.matchar.2009.06.007